Electronic Materials Letters, Vol. 9, No. 4 (2013), pp. 375-379
DOI: 10.1007/s13391-013-0003-7

PEDOT:PSS-Free Organic Photovoltaic Cells Using Tungsten Oxides as Buffer Layer on Anodes

Il Soo Oh, Gyu Min Kim, Seong Hun Han, and Se Young Oh*

Department of Chemical and Biomolecular Engineering, Sogang University, Seoul 121-742, Korea

(received date: 15 October 2012 / accepted date: 9 January 2013 / published date: 10 July 2013)

Tungsten oxide (WO_3) was used as an anode buffer layer in conventional poly(3-hexylthiophene):[6,6]-phenyl C61 butyric acid methyl ester (P3HT:PCBM-60) bulk hetero junction (BHJ) cells. Such a buffer layers acts as a hole-extraction layer and reduce series resistance, which leads to better performance of organic electronic devices. Organic photovoltaic (OPV) cells consisting of ITO/WO_3/P3HT:PCBM/Al were fabricated. Photovoltaic devices with a short-circuit current density of 7.77 mA/cm^2, an open-circuit voltage of 6.1 V, and a power conversion efficiency of 2.61% were achieved. This study revealed that WO_3 based cells have significant shunt resistance which contributes to a high fill factor and open-circuit voltage. This demonstrates potential for using WO_3 in poly(stylenesulfonate) doped poly(3,4-ethylenedioxythiophene):(PEDOT:PSS)-free systems.

Keywords: organic photovoltaic cell, tungsten oxide, anode buffer, impedance spectroscopy

1. INTRODUCTION

Organic photovoltaic (OPV) cells have attracted considerable attention in recent years for their flexibility and potential to achieve low-cost solar energy harvesting. In conventional OPV devices, poly(stylenesulfonate) doped poly(3,4-ethylenedioxy-thiophene):(PEDOT:PSS) films are used as buffer layers between the anodes. The advantage of incorporating PEDOT:PSS buffer layers in OPV devices from several properties that is closely related to its beneficial use in organic light emitting diodes (OLEDs).[1] PEDOT:PSS planarizes the indium tin oxide (ITO) surface by smoothening surface imperfections and reducing the root-mean-square roughness from 10 nm for bare ITO to 3 nm for a 50 nm layer of PEDOT:PSS on ITO.[2] The work function of PEDOT:PSS is on the order of 5.0 - 5.2 eV[3,4] which leads to a built-in potential of 0.8 - 1.0 V when combined with aluminium (Al) cathodes (4.2 eV) according to the simplifying metal-insulator-metal (MIM) model.[5-7] Although there are advantages of introducing a PEDOT:PSS layer in OPVs, various obstacles related to this buffer layer have also been reported, with focus on the acidity of the aqueous dispersions and the water uptake of solid films. The acidity of PEDOT:PSS in the pH range of 1-2 is suspected to dissolve indium ions from the ITO layer, which migrate from the anode into the buffer layer and even contaminate the photoactive layer.[8,9] When thoroughly dried, layers of PEDOT:PSS will uptake water again if they are left unprotected in the presence of air. The release of water in a functional device is considered to be a severe source of degradation, as water might corrode the metallic contacts or possibly oxidize the adjacent semiconductor organic layer.

Various modifications of PEDOT:PSS have been discussed as alternative buffer layers in OPVs. Other hole-injection polymers with larger work functions have been made to enhance hole injection.[10,11] Large work function hole injection polymers have resulted in reduced operating voltage as well as lifetime enhancement.[12] PEDOT:PSS, copper phthalocyanine (CuPc), and thin evaporated gold (Au) films were compared in parallel as buffer layers in bulk-heterojunction (BHJ) OPVs by Yoo *et al*.[13] A significant increase for open-circuit voltage and efficiency was found in regard to the organic layers in contrast to bare ITO or Au. Inorganic layers of transition metal oxides have been discussed as an alternative to PEDOT:PSS, such as vanadium (III) oxide (V_2O_3) and molybdenum oxide (MoO_3) vacuum deposited onto the ITO in OPVs.[14] Tao *et al*. employed a low-cost, non-toxic, and easily evaporable tungsten oxide (WO_3) as a buffer layer between the photoactive layer and top electrode in inverted polymer solar cells.[15] Although this approach improves performance, it has a limited role in buffer layers.

The purpose of this study is to describe and examine WO_3 in replacement of PEDOT:PSS as an anode buffer layer in the conventional poly(3-hexyl-thiophene):[6,6]-phenyl C61 butyric acid methyl ester (P3HT:PCBM-60) BHJ cells. This paper mainly introduces the performances of OPV cells

*Corresponding author: syoh@sogang.ac.kr

using WO_3 buffer layers by thermal evaporation on the ITO in comparison to standard PEDOT:PSS cells. We investigated the novel physical and electrical structural properties of the OPV cells using measurements of current-voltage and impedance spectroscopy.

2. EXPERIMENTAL PROCEDURE

Organic photovoltaic cells consisting of ITO/WO_3/P3HT:PCBM/Al were fabricated with an active surface area of 4 mm^2. Before the deposition of each layer, a patterned ITO (≤20 Ω/□) glass substrate was immersed in an ultrasonic bath of deionized water, acetone and isopropyl alcohol for 15 min for each solvent respectively. Then, the cleaned ITO glass substrate was dried at 80°C for 60 min in a vacuum oven. After a UV-ozone treatment for 15 min, a mixture solution of PEDOT-PSS was spin-casted onto the cleaned ITO glass substrate at 5000 rpm for 40 sec, followed by drying at 150°C for 10 min in a vacuum oven. Thin films of WO_3 (purchased from Sigma-Aldrich) were thermally evaporated in a high vacuum under 10^{-6} Torr onto ITO films on glass substrates. After deposition of the WO_3 layers, a solution of P3HT:PCBM (1 : 0.8) in chlorobenzene (18 mg/mL) was spin-casted onto the WO_3 layer at 1500 rpm. Finally, the Al cathode electrode (1000 Å) was deposited using a thermal evaporation technique under 10^{-6} torr. The prepared photovoltaic cell was then annealed at 150°C for 10 min. The OPV cells developed here were fabricated in atmospheric conditions except for the evaporation process. Power conversion efficiency was measured under simulated AM 1.5 solar illumination at 100 mW/cm^2 (one sun) using a solar simulator (Newport 69920, Newport Co., Ltd., USA). Impedance spectroscopy was obtained with IVUMSTATE (Spectra Pro 300i, Acton research Co., Ltd., USA).

3. RESULTS AND DISCUSSION

In earlier studies, attempts were made to substitute PEDOT:PSS as the buffer layer in OPV cells. Tao *et al.* suggested that the transition metal oxides can effectively substitute PEDOT:PSS as the buffer layer in OPV cells. In this study we explored the WO_3 layer as an anode buffer in conventional P3HT:PCBM-60 BHJ cells with special attention paid to the series resistance as well as device performance. The device architecture is shown schematically in Fig. 1(a) for solar cells made in a structure of ITO/WO_3 or PEDOT:PSS/P3HT:PCBM-60/Al. The energy level diagrams of the different materials used in the device fabrication are shown in Fig. 1(b). The high work function of WO_3 was 4.8 eV, which is suitable for transporting holes. It is expected that WO_3 as an anode buffer spacer would be effective in improving the performance of OPV cells due to a decrease of series resistance.

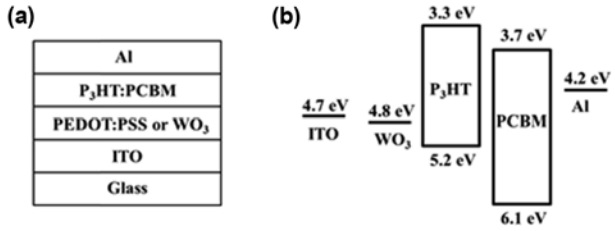

Fig. 1. (a) Structure of OPV cells consisting of WO_3 buffer layers and (b) energy level diagram of OPV cells.

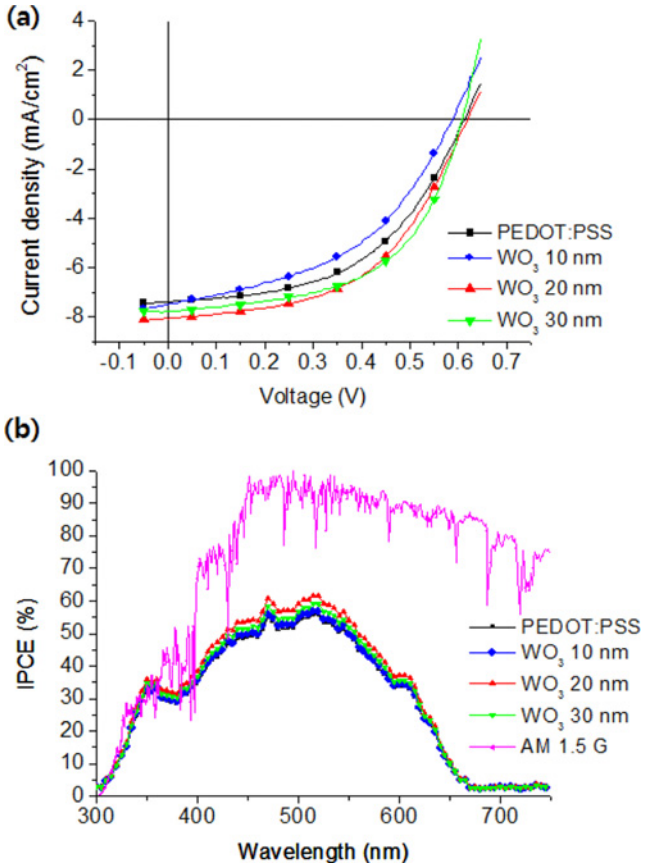

Fig. 2. (a) *J-V* Characteristics and (b) IPCE spectra under 100/cm^2 white light illumination in air for devices with different thicknesses of WO_3 used as a buffer layer between ITO and the active layer.

Figure 2(a) shows the current density-voltage (*J-V*) characteristics of the device with PEDOT:PSS and WO_3 under 100 mW/cm^2 white light illumination. The best device with 30 nm thick WO_3 exhibited a PCE of 2.61% and FF of 0.55, while the best device fabricated in the same batch with PEDOT:PSS exhibited a PCE and FF of 2.27% and 0.50, respectively.[16] The integrated IPCE and the I_{sc} measured on the same device, shown in Fig. 2(b), agree to within approximately 5%. Note that as the IPCE for PEDOT:PSS is limited to a lower fraction of the solar spectrum, higher efficiencies are anticipated for the WO_3 devices.

Table 1. Short-circuit current density (Jsc), open-circuit voltage (Voc), fill factor (FF), and power conversion efficiency (PCE) of devices according to the thickness of WO_3.

	Jsc (mA/cm²)	Voc (V)	FF	PCE (%)
PEDOT:PSS	7.39	0.61	0.50	2.27
WO_3 (10 nm)	7.49	0.59	0.45	1.99
WO_3 (20 nm)	8.08	0.62	0.51	2.54
WO_3 (30 nm)	7.77	0.61	0.55	2.61

$$J = J_{ph} - J_0(\exp^{q(V-JR_s)/nkT} - 1) - \frac{V+JR_s}{R_{SH}}. \quad (1)$$

The bulk resistance of the active materials and the contact resistance contribute to the series resistance. The contact resistance originates from the interface between the photoactive layer and electrodes. The series resistance defined by the slope of the *J-V* curve at $J = 0$ mA/cm^2, is estimated to be ~23.7 and ~14.0 Ω cm^2 for the devices with PEDOT:PSS and WO_3, respectively. Although most of the carriers are generated in the photo active layer, their collection is relative to the contact resistance at the organic/electrode interface. The decrease in series resistance indicates that the insertion of the thin WO_3 suppresses the contact resistance remarkably. The decrease in series resistance of from 23.7 to 14.0 Ω cm^2 contributes partly to the increase in FF. Meanwhile, the shunt resistance, defined by the slope of the *J-V* curves near 0 V under illumination, is estimated to be ~285 and ~464 Ω cm^2 for the devices with PEDOT:PSS and WO_3, respectively. The elevated shunt resistance also contributes to the improvement in FF. It is necessary for the WO_3 interfacial layer to cover the active layer fully and uniformly to reduce the current leakage. However, introducing a WO_3 layer will generally contribute to the series resistance using a lower current. Therefore, the effect of the WO_3 film thickness on device performance was investigated and is shown in Fig. 2. The detailed result is summarized in Table 1. When the thickness of WO_3 is 10 nm or less, the active layer will not be fully covered by WO_3, which tends to form some small islands instead of a uniform film.

Figure 3 shows the transmittance spectra of WO_3/ITO and PEDOT:PSS/ITO substrates. The transmittance by WO_3 was measured higher from the 370 nm to 500 nm range than PEDOT:PSS and slightly lower from the 500 nm to 600 nm range than PEDOT:PSS. This indicates that WO_3 films have potential to enhance optical properties of OPV cells as an optical spacer such as a TiOx layer. The fact that the cell performance does not show a significant dependence on the thickness of WO_3 layers may be beneficial in optimizing the optical and electrical structure of OPV cells. For example, we can vary the thickness of WO_3 layers without a significant compromise in cell electrical properties until the optical absorption by active layers is maximized with the help of multilayer thin-film optics[17] as in the work by Kim *et al.*[18] in which TiOx buffer layers also function as an optical spacer.

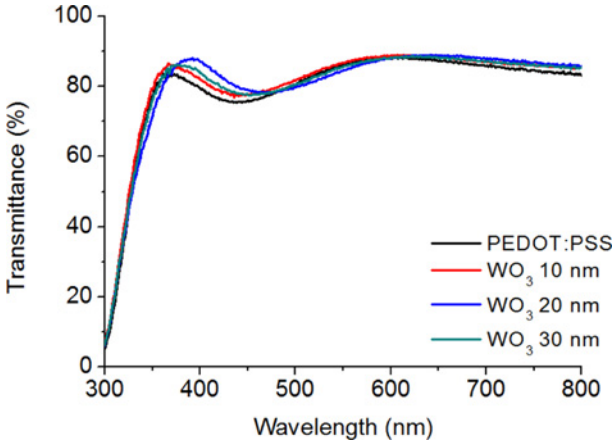

Fig. 3. Transmittance of WO_3/ITO and PEDOT:PSS/ITO substrates.

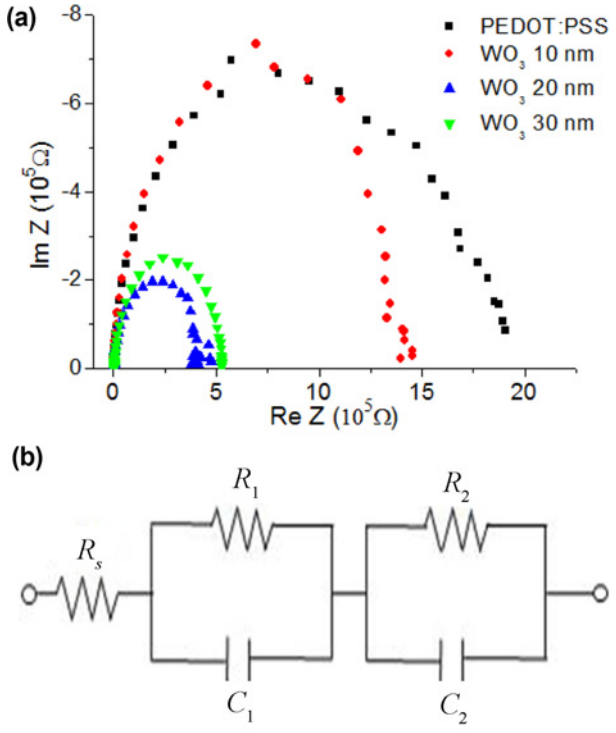

Fig. 4. (a) Impedance cole-cole plots for devices fabricated on ITO with WO_3 and (b) equivalent circuit model used for physical investigations of the impedance.

Figure 4(a) shows the impedance Cole-Cole plot for the devices fabricated on the ITO surface using buffer layers such as WO_3 and PEDOT:PSS. The horizontal and the vertical axes represent the real (Z') and the imaginary (Z'') parts of the impedance of the devices, respectively. The impedance for the devices is lowered significantly by the WO_3 anode buffer. The reduction of impedance can be

Table 2. Comparison of resistance and capacitance values for devices according to the thickness of WO_3.

	Rs (Ω)	R_1 (kΩ)	C_1 (nF)	R_2(kΩ)	C_2 (nF)
PEDOT:PSS	61.8	458	2.3	1309	4.34
WO_3 (10 nm)	41.7	1.74	13.5	1386	2.01
WO_3 (20 nm)	46.7	0.93	10.1	413	2.38
WO_3 (30 nm)	50.3	1.87	11.3	505	3.94

attributed to the smoothing morphology of the ITO surface and relatively high hole mobility of the WO_3 layers. For the purpose of constructing an equivalent circuit model for OPV cells, the impedance of the device was measured in the range of 10 Hz to 30 MHz at zero bias voltage. The results were analyzed using the following complex impedance equation:[19]

$$Z = \frac{1}{Y} = R + jX = R + \frac{1}{jwC} = Z' + jZ' \quad (2)$$

where Z, Y, R, X and C are the impedance, admittance, resistance, reactance, and capacitance of the device, respectively.

The equivalent circuit of these devices consists of a series resistance (R_1, R_2) and a capacitor (C_1, C_2) network in series with a contact resistance (R_S). This paper shows the equivalent electrical circuit for a two layered structure, where the WO_3 is the hole-transporting layer and P3HT:PCBM is the photo active layer, which consists of two parallel RC circuits connected in series, as shown in Fig. 4(b). The simulated results of this equivalent circuit model are in strong agreement with the experimental results. The values of the contact resistance (R_S), the series resistances (R_1, R_2), and the parallel capacitances (C_1, C_2) extracted from the frequency-dependent real and imaginary parts of the impedance of the devices with WO_3 and PEDOT:PSS are summarized in Table 2. The reduction of the barrier height is attributed to an increase in C_1. The reduction in the driving voltage is attributed to a reduction in the R_1 of devices with WO_3, which is well supported by our impedance spectroscopy analysis.

The deposition of a thin 10 nm thick WO_3 layer on the ITO is shown to yield a highly smooth surface with a RMS roughness as small as 0.88 nm.[16] This RMS roughness is comparable to that of PEDOT:PSS (= 0.81 nm) spun on ITO and much smaller than that of a bare ITO surface (= 2.8 nm), while the RMS of 10 nm thick WO_3 is slightly higher than PEDOT:PSS. We found that a RMS of 20 nm and 30 nm thick WO_3 is more uniform than the RMS of 10 nm thick WO_3. We believe that morphology properties influence series resistances and capacitances of OPV cells. The smoothing effect of WO_3 is expected to reduce the chance of direct shorts and local high fields, thus helping prevent leakage current and formation of defects that can be induced by the above factors.

4. CONCLUSIONS

In summary, we have proposed and successfully achieved a promising approach to elaborate a PEDOT:PSS free multilayer system using WO_3 as a buffer layer. The photovoltaic cells exhibit a better performance buffer layer and diode properties with WO_3. In addition, an important J_{sc} of 7.77 mA/cm^2 and a maximum efficiency of 2.61% were reached. Using WO_3 the efficiency of the devices was particularly enhanced by high FF due to improved hole mobility across the WO_3 layer. Further work is necessary to improve the charge carrier transport through the buffer layer and to fully benefit from the WO_3 implementation in the device structure. The smoothness of WO_3 layers and the improved hole mobility of P_3HT films grown on WO_3 are also expected to benefit OPV cells by reducing the chance of bias dependent carrier recombination.

ACKNOWLEDGEMENTS

This work was supported by a Human Resource Development of the Korea Institute of Energy Technology Evaluation and Planning (KETEP) grant funded by the Korea Government Ministry of Knowledge Economy (No.20114010203090), and a National Research Foundation of Korea (NRF) grant funded by Korean Ministry of Education, Science, and Technology (MEST) (No.20120002171).

REFERENCES

1. T. W. Lee, K. G. Lim, and D. H. Kim, *Electron. Mater. Lett*. **6**, 41 (2010).
2. C. Jonda, A. B. R. Mayer, U. Stolz, A. Elshner, and A. Karbach, *J. Mater. Sci.* **35**, 5645 (2000).
3. T. M. Brown, J. S. Kim, R. H. Friend, F. Cacialli, R. Daik, and W. J. Feast, *Appl. Phys. Lett.* **75**, 1679 (1999).
4. J. S. Kim, R. H. Friend, and F. Cacially, *Appl. Phys. Lett*. **74**, 3084 (1999).
5. I. D. Parker, *J. Appl. Phys.* **75**, 1656 (1994).
6. G. G. Malliaras, J. R. Salem, P. J. Brock, and J. C. Scott, *J. Appl. Phys.* **84**, 1583 (1998).
7. A. Shahini and K. Abbasian, *Electron. Mater. Lett.* **8**, 435 (2012).
8. M. P. de Jong, L. J. van Ijzendoorn, and M. J. A. de Voigt, *Appl. Phys. Lett*. **77**, 2255 (2000).
9. J. K. J. van Duren, J. Loos, F. Morrissey, C. M. Leewis, K. P. H. Kivits, L. J. van IJzendoorn, M. T. Rispens, J. C. Hummelen, and R. A. J. Janssen, *Adv. Func. Mater*. **12**, 665 (2002).
10. S. Kim, C. Hsu, C. Zhang, H. Skulason, F. Uckert, D. LeCoulux, Y. Cao, and I. Parker, *J. Soc. Inf. Disp*. **5**, 14 (2004).
11. K. R. Choudhury, J. W. Lee, N. Chopra, A. Gupta, X. Z.

Jiang, F. Amy, and F. So, *Adv. Funt. Mater*. **19**, 491 (2009).
12. T. W. Lee, M. G. Kim, S. Y. Kim, S. H. Park, O. Kwon, T. Noh, and T. S. Oh, *Appl. Phys. Lett*. **89**, 123505 (2006).
13. I. Yoo, M. Lee, C. Lee, D. W. Kim, I. S. Moon, and D. H. Hwang, *Synth. Met*. **153**, 97 (2005).
14. K. Hong and J. L. Lee, *Electron. Mater. Lett*. **7**, 77 (2011).
15. C. Tao, S. Ruan, G. Xie, X. Kong, L. Shen, F. Meng, C. Liu, X. Zhang, W. Dong, and W. Chen, *Appl. Phys. Lett.* **94**, 043311 (2009).
16. S. C. Han, W. S. Shin, M. S. Seo, D. Gupta, S. J. Moon, and S. H. Yoo, *Organic Electronics* **10**, 791 (2009).
17. L. A. A. Pettersson, L. S. Roman, and O. Inganas, *J. Appl. Phys.* **86**, 487 (1999).
18. J. Y. Kim, S. H. Kim, H. H. Lee, K. Lee, W. Ma, X. Gong, and A. J. Heeger, *Adv. Mater.* **18**, 572 (2006).
19. J. R. Macdonald, *Impedance Spectroscopy-Emphasizing Solid Materials and Systems,* p. 15, John Wiley & Sons, New York (1987).